Materials Letters 93 (2013) 88–91

Contents lists available at SciVerse ScienceDirect

Materials Letters

journal homepage: www.elsevier.com/locate/matlet

Fabrication of wrinkled Nb-doped TiO_2 nanofibres via electrospinning

HyeLan An, Hyo-Jin Ahn *

Department of Materials Science and Engineering, Seoul National University of Science and Technology, Seoul 139-743, Republic of Korea

ARTICLE INFO

Article history:
Received 11 June 2012
Accepted 17 November 2012
Available online 27 November 2012

Keywords:
Electrospinning
Wrinkled nanofibers
Nb-doped TiO_2 (NTO)
Formation mechanisms

ABSTRACT

Nb-doped TiO_2 (NTO) nanofibres (NFs), ranging from cylindrical NFs to wrinkled NFs, were synthesised using an electrospinning method. Mechanisms leading to the formation of structures with different properties were demonstrated. In order to synthesise wrinkled NTO NFs, the mole ratios of the Nb precursor to the Ti precursor were controlled to be 0, 0.09, 0.23, 0.38, and 0.59. The NTO NFs prepared from the mole ratio of 0.59 had an excellent wrinkled structure with a high specific surface area and phase transformation from an anatase structure to a rutile structure.

© 2012 Elsevier B.V. All rights reserved.

1. Introduction

Recently, one-dimensional (1-D) nanostructures have attracted great attention because of their peculiar optical, electrical, chemical, and electrochemical properties, as well as their uses in various applications such as biodiagnostics, electrochemistry, optics, and electronics [1,2]. Much effort has been made to fabricate 1-D nanostructures with various morphologies, such as multi-segment nanowires (NWs), nanorods, hollow NWs, core–shell NWs, and branched NWs [1,3–5]. Various synthetic methods, such as template-directed synthesis, lithography, chemical vapour deposition, vapour phase synthesis, and electrospinning, have been developed in order to obtain such 1-D nanostructures [5–7]. Among these methods, electrospinning, which produces very fine fibres in the range 20–1000 nm, is a very attractive technique for making 1-D nanostructures with various morphologies. This method is used in bio-pharmaceuticals, filters, sensors, electronics/photovoltaics, and energy-conversion systems because of its advantages such as cost effectiveness, good repeatability, control of fibre dimensions, and large-scale production [8]. The morphologies of 1-D nanostructures can have direct effects in the above-mentioned applications and, by extension, the morphological modification of 1-D nanostructures by electrospinning has become an important issue. For example, Li et al. reported the fabrication of TiO_2 hollow nanofibres (NFs) through co-electrospinning using two immiscible liquids [9]. Kurban et al. controlled the morphologies to give porous fibres and cylindrical fibres via co-electrospinning together with a solvent-selection system, for use in hydrogen-storage materials [10]. An et al. recently reported the synthesis of carbon NF (CNF) composites consisting of SnO_2 and SiO_2 nanoparticles by co-electrospinning; the CNF nanocomposites had a rough and dense surface, which could be controlled by varying the weight percentage ratios of SnO_2 and SiO_2 nanoparticles [11]. In addition, among various transparent conductive oxides (TCOs) such as Sn-doped In_2O_3 (ITO) and F-doped SnO_2 (FTO), Nb-doped TiO_2 (NTO) materials have been receiving much attention as promising TCO materials because of their low resistivities (9.5×10^{-4} and $2–3\times10^{-4}\,\Omega$ cm) and high transmittances (60–85% and 77–97% in the visible region) using sputtering and pulsed laser deposition [12,13]. However, wrinkled NTO NFs have not yet been reported.

In this study, we successfully synthesised wrinkled NTO NFs by an electrospinning technique. We discuss the mechanisms leading to the formation of different morphologies, ranging from cylindrical NFs to wrinkled NFs.

2. Experiments

Titanium (IV) isopropoxide ($Ti[OCH(CH_3)_2]_4$, Aldrich, 97%), poly (vinylpyrrolidone) ($(C_6H_9NO)n$, $M_w=1\,300\,000$ g/mol, Aldrich), and acetic acid (CH_3CO_2H, Aldrich, 99.7%) were dissolved in N,N-dimethylformamide ($HCON(CH_3)_2$, Aldrich, 99%) by stirring for 1 h. Niobium (V) ethoxide ($Nb(OCH_2CH_3)_5$, Aldrich, 99.9%) was then added to the Ti precursor solution. In order to obtain wrinkled NTO NFs, the relative mole ratios of the Nb to the Ti precursor were controlled to be 0, 0.09, 0.23, 0.38, and 0.59 (referred to as single TiO_2 NFs, and samples A–D). The as-prepared solution was loaded into a 12 mL standard syringe equipped with a 23-gauge stainless-steel needle. The feeding rate was fixed at 0.04 mL/h, using a syringe pump. The voltage of the power supply was ~14.5 kV. The distance between the needle tip and the collector was maintained at ~20 cm. All of the as-spun samples were heat-treated at 500 °C

* Corresponding author. Tel.: +82 02 970 6622; fax: +82 02 973 6657.
E-mail address: hjahn@seoultech.ac.kr (H.-J. Ahn).

0167-577X/$ - see front matter © 2012 Elsevier B.V. All rights reserved.
http://dx.doi.org/10.1016/j.matlet.2012.11.066

for 5 h in air. We obtained NTO NFs with a range of morphologies, such as cylindrical NFs and wrinkled NFs.

The structures and crystallinities of the samples were examined using X-ray diffraction (XRD, Rigaku Rint 2500) with Cu K_α radiation in the range of 10–90°. The morphological changes and structural properties of the samples were investigated using field-emission scanning electron microscopy (FESEM, Hitachi S-4700) and transmission electron microscopy (TEM, JEOL-2100F, KBSI Suncheon Center) operated at 200 kV. The surface areas of the NFs were measured using the Brunauer–Emmet–Teller (BET, Micromeritics ASAP2010) method.

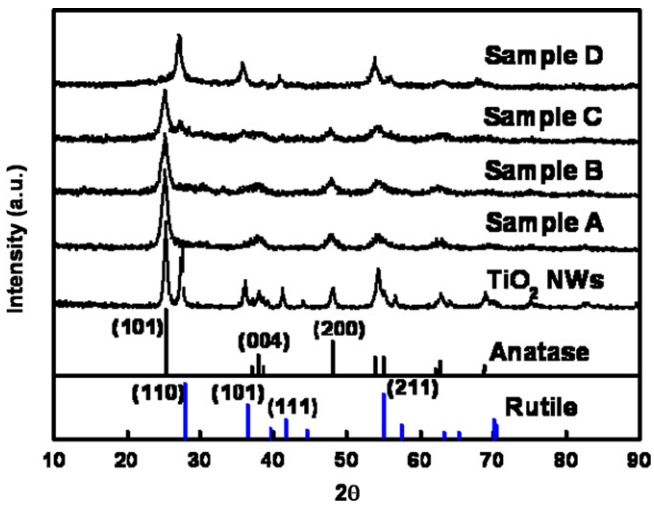

Fig. 1. XRD data of single TiO_2 NFs, and samples A–D after calcination.

3. Results and discussion

Fig. 1 shows the XRD patterns of single TiO_2 NFs, and of samples A–D, obtained after calcination. In the case of the single TiO_2 NFs, XRD peaks were observed at 25.3°, 37.8°, 48.0°, 53.9°, 62.7°, and 68.8°, corresponding to the (101), (004), (200), (105), (204), and (116) planes of anatase TiO_2 phases (JCPDS no. 841286) and at 27.9°, 36.4°, 41.7°, and 55.1°, corresponding to the (110), (101), (111), and (211) planes of rutile TiO_2 phases (JCPDS no. 881175). For samples A–C, the XRD peaks indicate that the anatase TiO_2 phases decreased gradually as the amount of Nb doping increased, and the diffraction peaks relative to the (101) planes of samples A–C shifted gradually to lower 2θ values with increasing amounts of Nb doping; this is because the ionic radius of Nb^{5+} (0.62 Å) is bigger than that of Ti^{4+} (0.56 Å), and can be explained using the Bragg equation ($\lambda = 2d \sin\theta$). In particular, sample D shows that at a critical level of Nb doping, phase transformation from anatase TiO_2 to rutile TiO_2 occurred, as shown in Fig. 1. This phenomenon could be explained as grain growth suppression in the NFs as a result of the critical amount of Nb doping, which implies preferential growth orientation of the NFs [14].

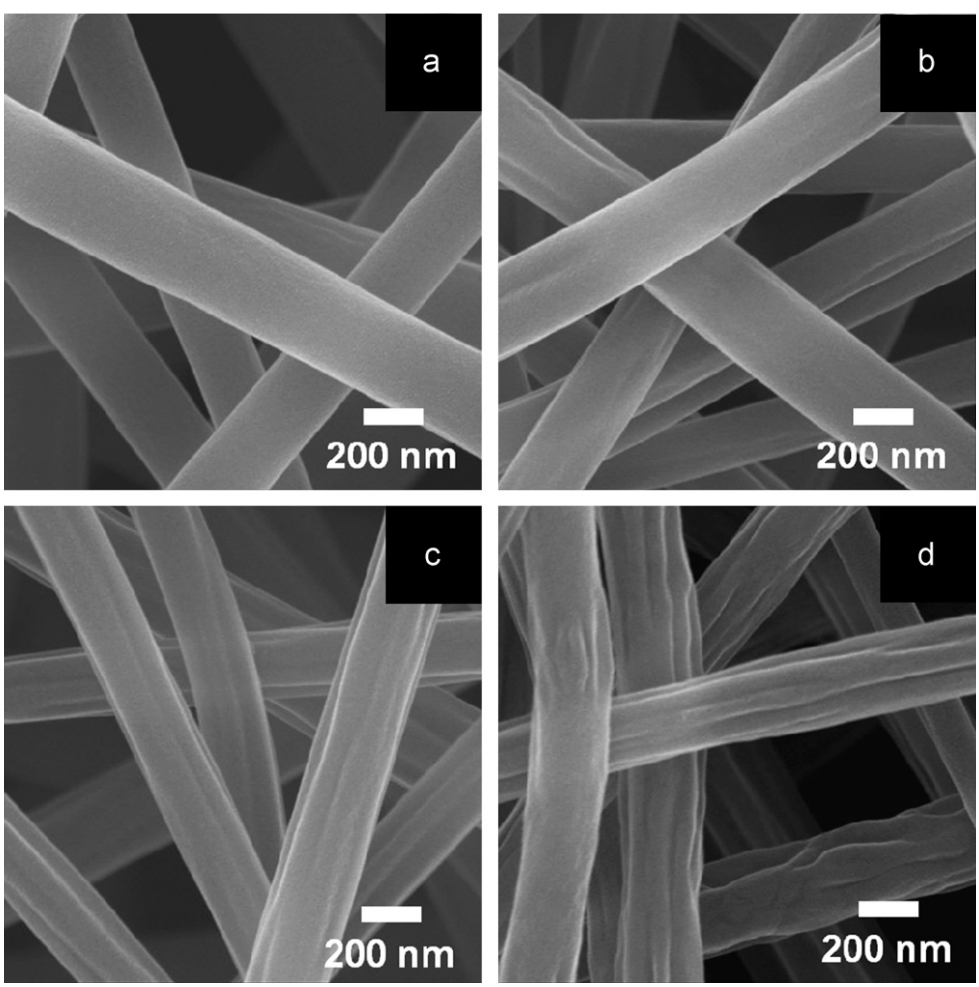

Fig. 2. SEM images of as-spun samples A–D (a–d) before calcination.

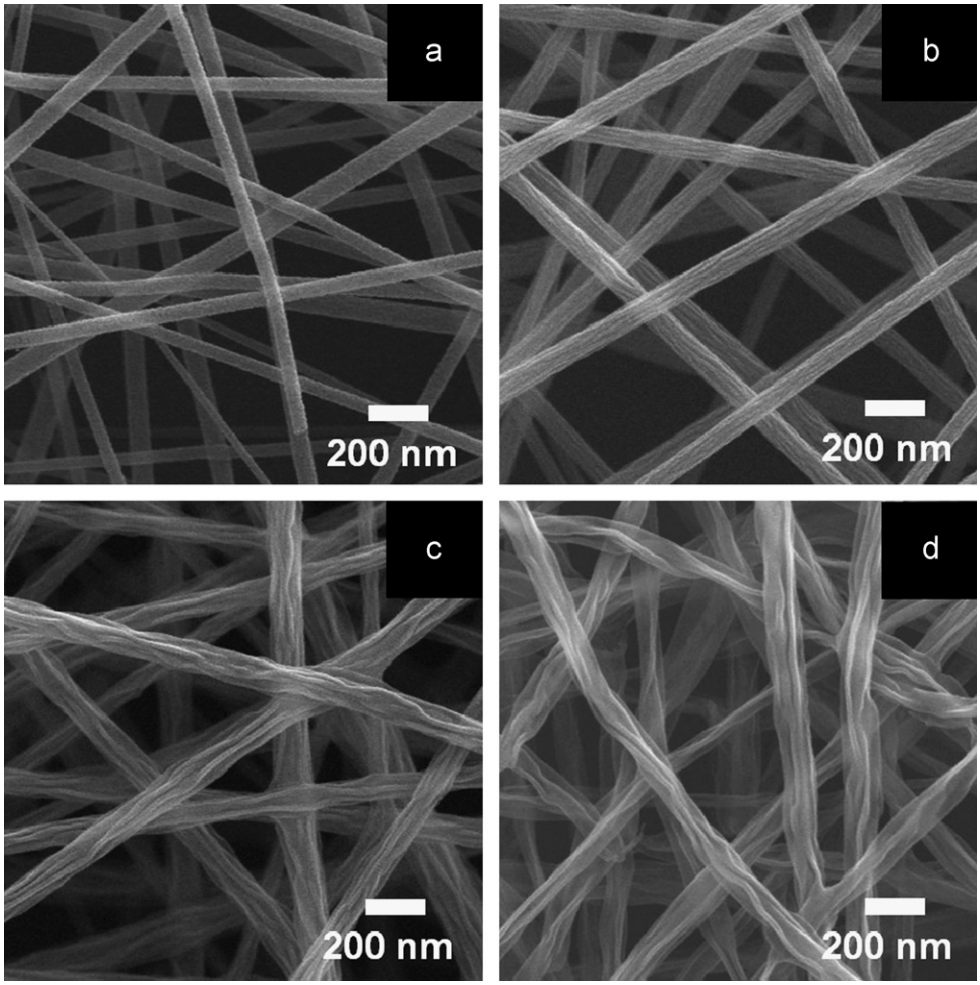

Fig. 3. SEM images of samples A–D after calcination.

Fig. 2(a)–(d) shows the SEM images of as-spun samples A–D. These samples consist of precursors and PVP polymer composite NFs. Interestingly, samples C and D have a rough NF surface compared to samples A and B. Therefore, the wrinkled NFs are formed before calcination, as shown in Fig. 2(c) and (d).

Fig. 3(a)–(d) shows the SEM images of samples A–D, obtained after calcination at 500 °C. The diameters of the NFs are in the range ~41–79 nm for sample A, ~55–90 nm for sample B, ~79–122 nm for sample C, and ~80–134 nm for sample D. Interestingly, in terms of NF morphology, the results show that NTO NFs transform systematically from cylindrical NFs (Fig. 3(a)) to wrinkled NFs (Fig. 3(d)) with increasing Nb doping; samples A and B exhibit relatively smooth NTO NF surfaces, while samples C and D exhibit rough NTO NF surfaces, with a high surface area. In general, TiO_2 NFs of diameter 100 nm have specific surface areas of ~20 m^2/g. For the wrinkled NTO NFs, the BET surface areas were measured using nitrogen adsorption. It was shown that the specific surface area increased with increasing levels of Nb doping. The BET surface area was 87.3 m^2/g for sample A and 126.5 m^2/g for sample D. These results indicate that the specific surface areas of samples A and D increased 4.38-fold and 6.32-fold compared to that of single TiO_2 NFs fabricated by electrospinning.

Fig. 4(a)–(d) presents the TEM images of samples A, B, and D, obtained after calcination. All the samples were composed of small nanoparticles from ~3 to ~6 nm in size. The TEM measurements clearly show that sample A (Fig. 4(a) consisted of uniformly cylindrical NFs and sample D (Fig. 4(d)) consisted of wrinkled NFs. To confirm the crystalline planes or crystal periodicities of the NFs, enlarged HRTEM images from samples A and B were obtained, and are shown as insets in Fig. 4(a) and (d). Sample A, as shown in the inset of Fig. 4(a), was observed to contain the (101) plane of the anatase TiO_2 phase with a lattice distance of ~3.52 nm, which implies successful formation of anatase TiO_2 phases. In the case of sample D, the (110) plane of the rutile TiO_2 phase with a lattice distance of ~3.20 nm was observed, which implies successful formation of rutile TiO_2 phases. Electron diffraction patterns were obtained to further demonstrate the crystal structures of samples A and D. Sample A shows the (101), (004), (200), and (105) planes, as seen in the left of Fig. 4(e), and sample D shows the (110), (101), (111), and (211), as seen in the right of Fig. 4(e). In addition, the (110) plane of Nb was observed in samples A and D. HRTEM results are therefore in good agreement with the XRD results. In order to confirm the distribution of Nb and Ti atoms in the NFs of sample D, EDS mapping was carried out. The results indicated that Nb and Ti atoms were uniformly distributed in the NFs. Furthermore, the EDS results of the samples showed that the compositions of Nb and TiO_2 are 10.9 and 89.1 wt% for sample A, 20.7 and 79.3 wt% for sample B, 29.7 and 70.3 wt% for sample C, and 38.6 and 61.4 wt% for sample D, respectively.

We successfully fabricated wrinkled NTO NFs with a high specific surface area. The mechanism of formation of wrinkled NTO NFs is directly related to the morphology of the as-spun NTO NFs before calcination. We believe that the wrinkled morphology of sample D is the result of agglomeration of two different

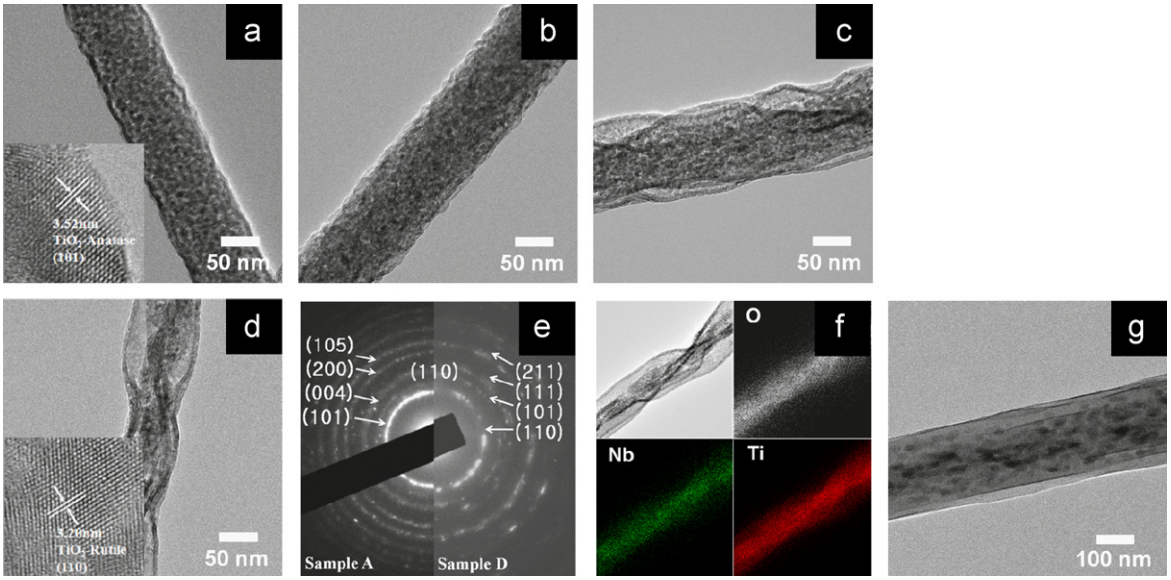

Fig. 4. TEM images (a–d) of samples A–D, EDP patterns (e) of samples A and D, and TEM–EDS mapping data (f) and as-spun TEM images (g) obtained from sample D.

precursors linked by PVP in the as-spun NFs (Fig. 4(g)) and of the buckling effect of a cylindrical polymer shell, arising from removal of solvent during the electrospinning process [15]. Wrinkled NTO NFs with high specific surface areas are successfully formed as a result of the optimum amount of Nb doping. Wrinkled NTO NFs can therefore be used directly in applications (e.g. as catalyst supports, TCO materials, and solar cells) requiring 1-D nanostructures with high surface areas.

4. Summary

Wrinkled NTO NFs with high specific surface areas were successfully fabricated via electrospinning and their formation mechanism and structural properties were demonstrated. The results indicated that NTO NFs with the optimum amount of Nb doping form a wrinkled morphology with a rutile structure and a high specific surface area.

Acknowledgement

This work was supported by Grant no. 10041161 from the Ministry of Knowledge Economy (MKE) and the Fundamental R&D Program for Core Technology of Materials funded by the Ministry of Knowledge Economy, Republic of Korea.

References

[1] Park S, Lim JH, Chung SW, Mirkin CA. Science 2004;303:348–51.
[2] Ahn HJ, Wang D. Solid State Sci 2011;13:1612–5.
[3] Li D, Xia Y. Adv Mater 2004;16:1151–70.
[4] An GH, Jeong SY, Seong TY, Ahn HJ. Mater Lett 2011;65:2377–80.
[5] Xia Y, Yang P, Sun Y, Wu Y, Mayers B, Gates B, et al. Adv Mater 2003;15:353–89.
[6] Banerjee N, Krupanidhi SB. J Alloys Compd 2013;547:147–51.
[7] Lipomi DJ, Chiechi RC, Dickey MD, Whitesides GM. Nano Lett 2008;8:2100–5.
[8] Rmakrishna S, Fujihara K, Teo WE, Lim TC, Ma Z. An introduction to electrospinning and nanofibers. Singapore: World Scientific Publishing Co. Ltd.; 2005.
[9] Li D, Xia Y. Nano Lett 2004;4:933–8.
[10] Kurban Z, Lovell A, Bennington SM, Jenkins DWK, Ryan KR, Jones MO, et al. J Phys Chem 2010;114:21201–13.
[11] An GH, Ahn HY. Ceram Int 2012;38:3197–201.
[12] Yamada N, Hitosugi T, Hoang NLH, Furubayashi Y, Hirose Y, Shimada T, et al. Appl Phys 2007;46:5275–7.
[13] Furubayashi Y, Hitosugi T, Yamamoto Y, Inaba K, Kinoda G, Hirose Y, et al. Appl Phys Lett 2005;86:252101.
[14] Arbiol J, Cerda J, Dezanneau G, Cirera A, Peiro F, Cornet A, et al. J Appl Phys 2002;92:853–61.
[15] Pai CL, Boyce MC, Rutledge GC. Macromolecules 2009;42:2102–14.